Clays and Clay Minerals, Vol. 46, No. 3, 270–279, 1998.

FORMATION OF VERMICULAR KAOLINITE FROM HALLOYSITE AGGREGATES IN THE WEATHERING OF PLAGIOCLASE

GI YOUNG JEONG

Department of Earth and Environmental Sciences, Andong National University, Andong 760-749, Korea

Abstract—Halloysite and kaolinite coexist in anorthosite weathering profiles in the Sancheong district, Korea. X-ray diffraction (XRD) analysis on a transect of partially weathered anorthosites reveals an increasing amount of kaolinite development with weathering age. Microtextures were examined by scanning electron microscopy (SEM) of thin sections and raw samples in an attempt to resolve the genetic relation between halloysite and kaolinite. In the earliest stage of weathering, halloysite ellipsoids and short tubes form on the plagioclase surfaces. The successive formation of new grains from the early grains results in globular aggregates where halloysite grains are partially interconnected. With the further progress of weathering, the halloysite grains coalesce from the inner part of the aggregate outward, and convert into stacked kaolinite plates. Continuous addition of halloysite grains on existing plates and their subsequent conversion into plates form long vermicular kaolinite. Solid-state transformation is suggested as a major conversion mechanism. Concurrently with its successive transformation into kaolinite, halloysite also continuously precipitates, giving rise to overgrowths on vermicular kaolinite. Halloysite forms as a kinetically favored metastable precursor and is subsequently transformed into thermodynamically stable kaolinite. Halloysite and kaolinite coexist temporarily in the weathering profile far from equilibrium.

Key Words—Halloysite, Kaolinite, Scanning Electron Microscopy, Weathering.

INTRODUCTION

Halloysite and kaolinite are important weathering products of rocks in temperate and tropical environments. Previous electron microscopic studies frequently reported the coexistence of both minerals in weathering profiles (Keller 1977; Gilkes et al. 1980; Keller et al. 1980; Banfield 1985; Banfield and Eggleton 1990). Their coexistence is of interest because they have similar chemistry and structure. The chemical composition of kaolinite is the same as that of halloysite except for weakly bound interlayer water (Weaver and Pollard 1973; Newman and Brown 1987), while the structure of halloysite differs from that of kaolinite in layer stacking sequence. Disordered kaolinite is hardly distinguishable from dehydrated halloysite (Chukhrov and Zvyagin 1966; Brindley 1980; Bailey 1990). A genetic relation between the 2 minerals in the weathering environment is rarely established, despite many reports describing their coexistence. Thermodynamic studies predict that halloysites would convert into kaolinite with aging (Huang 1974; Tsuzuki and Kawabe 1983), but while this sequence is currently accepted by most investigators (Parham 1969; Keller 1977; Nagasawa 1978; Churchman and Gilkes 1989; Steefel and Van Cappellen 1990), there is little direct microtextural evidence to support it. Banfield (1985), from SEM observations, suggested that halloysite tubes merged into platy kaolinite. Robertson and Eggleton (1991) and Singh and Gilkes (1992), in their transmission electron microscopic (TEM) studies, reported a conversion of kaolinite to halloysite in the kaolin pseudomorph after muscovite. More extensive microtextural study is required to elucidate the genetic relation between halloysite and kaolinite.

Residual kaolin formed by the weathering of anorthosite in the Sancheong district, Korea, consists mostly of halloysite and kaolinite (Jeong 1992; Jeong and Kim 1994). The microtextures of partially weathered anorthosites underlying kaolin record the sequential formation of the 2 minerals very well. Sancheong kaolin deposits are good sites to study the genetic relation between coexisting halloysite and kaolinite in the weathering environment. In the present study, microtextural changes of a series of partially weathered anorthosites were examined in detail, mainly using SEM to trace the genetic relation.

ANORTHOSITE AND KAOLIN DEPOSITS

Sancheong anorthosite is a monomineralic igneous rock composed mostly of medium- to coarse-grained labradorite plagioclase (normally above 95 vol%) with minor minerals such as amphiboles, chlorites, biotite, epidotes, muscovite, ilmenite and titanite (Jeong 1992). The Sm-Nd isotopic age of the anorthosite intrusion is 1,678 ± 90 Ma (Kwon and Jeong 1990). Microfractures are well developed in the anorthosite as a result of a cataclastic deformation during the regional metamorphism after the intrusion (Jeong and Lee 1987; Jeong and Kim 1993).

The kaolin deposits have been formed by residual weathering of the anorthosite under a humid temperate climate with mean annual precipitation of 1354 mm and mean air temperature of 12.7 °C (Jeong 1992; Jeong and Kim 1993). The kaolin deposits with annual production of about 0.2 million tons have been an important source of kaolin raw material for ceramics in Korea (Korea Mining Promotion Corporation 1995). The kaolins consist mostly of halloysite and kaolinite in vari-

Table 1. X-ray fluorescence analysis data of partially weathered anorthosites.

	Sample		
Wt%	R1	R2	R3
SiO_2	51.08	49.71	48.35
Al_2O_3	29.38	30.42	31.25
Fe_2O_3	0.53	0.51	0.48
MgO	0.31	0.37	0.25
MnO	0.01	0.01	0.01
TiO_2	0.08	0.09	0.08
P_2O_5	0.01	0.02	0.02
CaO	13.54	10.98	8.62
K_2O	0.29	0.28	0.41
Na_2O	3.44	3.00	2.54
Total	100.07	99.88	99.67

ous proportions (Jeong 1992; Jeong and Kim 1994). There is a gradual transition from fresh rock to kaolin across a thick zone of partially weathered rock. One of the remarkable characteristics of the anorthosite weathering profiles is good preservation of the original rock textures without severe disturbance: laminations, dykes, joints and small veins in the anorthosite extend throughout the weathering profiles without any noticeable change of orientation or width. Delicate textures of plagioclase grains, such as grain shape, cleavages and microfractures, are also well preserved even on the microscopic scale (Jeong and Kim 1993). Although it is very difficult to quantify precisely, volume change during the weathering appears to be small. Most of the deposits are found on mountainsides of low slope (less than 22°) that allow the development of thick weathering profiles ranging from 10 to 30 m in depth.

SAMPLES AND METHODS

Partially weathered anorthosite was sampled at the base of weathering profiles exposed at the excavation site in a kaolin quarry. Three partially weathered rock samples (R1, R2, R3) were collected at successive 20-cm intervals from the fresh anorthosite with increasing degree of weathering from R1 to R3 and stored in polyethylene bottles to preserve field moisture and original textures. The mineral composition of samples was determined with a Rigaku RAD3-C diffractometer equipped with Co X-ray tubes operating at 35 kV/20 mA. Bulk samples were lightly crushed in an agate mortar and packed in an aluminum holder. All the XRD analyses were carried out before drying of the samples. Since halloysite occurs as compact aggregates of fine tubular particles (Jeong and Kim 1993; this study), XRD pattern does not show significant orientation effects. A vermicular morphology of kaolinite in the samples also reduces the orientation effects compared to platy morphology. Therefore, the intensities of the basal peaks were reproducible sufficiently to show the relative variation of kaolin mineral contents in the samples. The bulk chemistry was determined with a Philips PW1480 X-ray fluorescence spectrometer at the Seoul branch of Korea Basic Science Institute. For a textural study, air-dried samples were impregnated with Araldite epoxy resin under vacuum. Polished thin sections were prepared from the resin-impregnated samples and coated with carbon. Weathered plagioclase grains were glued on to the aluminum stubs with conductive adhesives and coated with gold. The microtextures of thin sections and original samples were observed using a Hitachi S2500 scanning electron microscope. Thin sections were observed up to the maximum magnification of ×3000, and raw samples up to ×60,000. The chemistry of minerals was analyzed qualitatively with a Kevex energy dispersive X-ray spectrometer (EDS). A Philips CM20 transmission electron microscope equipped with a Link EDS system was used to observe the morphology of kaolin minerals and their aggregates. Samples were lightly dispersed in distilled water (without any severe treatment like ultrasonic agitation), loaded onto a copper grid covered with Formvar film and coated with carbon.

RESULTS

Bulk Chemistry and Mineral Composition of Weathered Anorthosites

The bulk chemistry of sample R1 simply reflects the chemistry of labradorite (An69%) (Table 1). The behavior of elements with increasing degree of weathering is generally consistent with the element mobility given in a geochemical text (Krauskopf and Bird 1995). CaO, Na_2O and SiO_2 systematically decrease toward sample R3, whereas Al_2O_3 increases slightly. Loss on ignition increases with progress of weathering, implying the formation of clays. Assuming that least-weathered sample R1 consists of 100 wt% plagioclase, the plagioclase content in sample R2 is calculated as 81 wt% and in R3 as 64 wt% on the basis of CaO content.

XRD patterns of bulk samples show the presence of 3 types of clay minerals: 15-Å, 10-Å and 7-Å phases (Figure 1). The 15-Å phase was previously identified as vermiculite by XRD (Mg saturation, ethylene glycol intercalation and heat treatments), SEM and electron microprobe analysis (Jeong 1992; Jeong et al. 1995). Vermiculite was formed by the early weathering of minor biotite. The second order reflection of mica is not observed at 5 Å. Therefore, the 10-Å phase is identified with 10-Å halloysite. Jeong and Kim (1992) carried out a systematic wet size fractionation study for kaolins (highly weathered anorthosite) composed of 10-Å and 7-Å phases from the same kaolin quarry. Mineralogical identification of the 9 size fractions ranging from 0.1 to 74 μm using XRD, SEM and TEM showed that the 10-Å phase in the finer fractions is mostly tubular halloysite, while the 7-Å phase in the coarser fractions is mostly vermicular kaolinite. The formamide intercalation test (Churchman et al. 1984) also gave results con-

https://doi.org/10.1346/CCMN.1998.0460306 Published online by Cambridge University Press

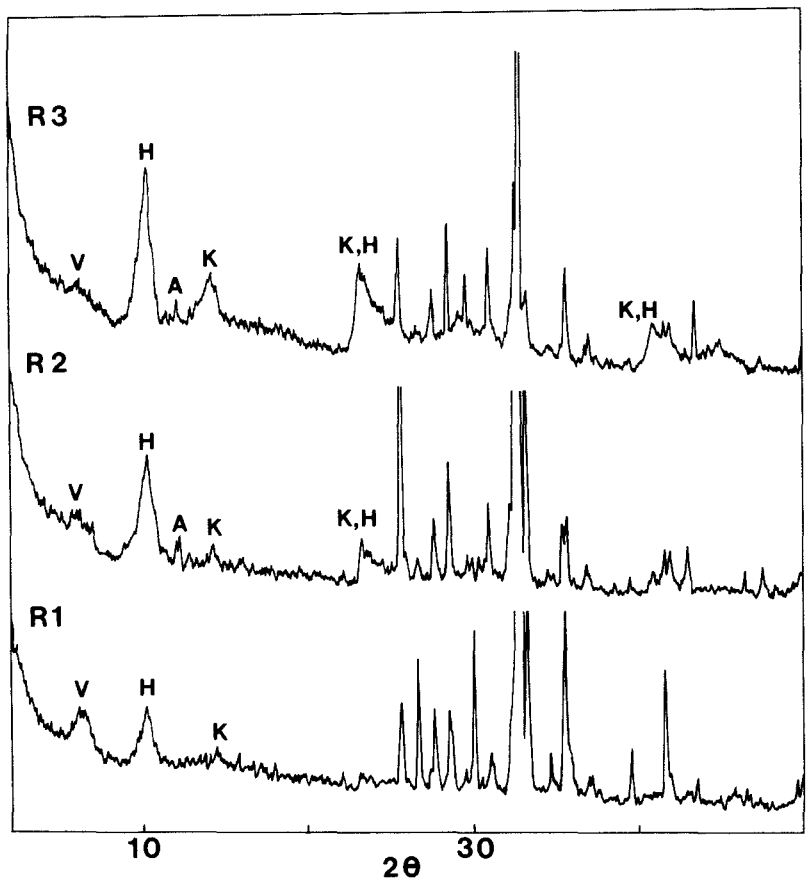

Figure 1. XRD patterns of samples R1, R2 and R3. Key: K = kaolinite; H = halloysite; V = vermiculite; and A = amphibole; nonmarked peak = plagioclase. Co$K\alpha$ radiation. Random mount of bulk powder samples.

sistent with those of XRD, SEM and TEM (Jeong and Kim 1992). Accordingly, the 10-Å and 7-Å phases in the kaolins and partially weathered anorthosites are 10-Å halloysite and kaolinite, respectively. The author's unpublished size fractionation data of kaolins from other kaolin quarries also confirmed that halloysite in the Sancheong district occurs as a hydrated form in the natural state. In the samples studied (Figure 1), 10-Å halloysite content steadily increases from sample R1 to R3. Kaolinite content is small in samples R1 and R2 but increases in sample R3. Measurement of the Hinckley index of kaolinite (Hinckley 1963) is very difficult because of the low kaolinite content of studied samples. The indices measured from other kaolinite-rich kaolins in the Sancheong district range from 0.4 to 0.6, implying low to moderate crystallinities (Jeong and Kim 1989). On the other hand, the crystallinity indices of Hughes and Brown (1979) range from 6.5 to 8.8, also implying low crystallinities. The basal peak of kaolinite is very broad and low, thus very similar to that of dehydrated halloysite (Figure 1). Jeong (1992) measured the relative intensity of diffraction peaks against corundum and showed that the relative intensity of the halloysite reflection at 10 Å is about 3 times that for an equivalent amount of kaolinite at 7 Å. Therefore, the halloysite-to-kaolinite ratio in sample R3 is estimated as about 1:1.

Microtextures of Weathered Anorthosite

SAMPLE R1. In the early stage of anorthosite weathering, microfractures in plagioclase are widened and partially filled with clays (Figures 2a and 2b). EDS analysis suggests that the clays are composed of kaolin minerals. Figure 2c shows the early development mode of kaolin mineral grains, which vary from tiny embryos (0.02 μm) to larger ellipsoids or irregular grains (0.3 μm). The irregular grains commonly have protuberances or spherical overgrowths. Spheres, ellipsoids and irregular grains constitute globular aggregates. A TEM photograph of the same sample (Figure 2d) shows ellipsoids with some tubes and spheres, all of which are confirmed as kaolin minerals by EDS analysis. The ellipsoids possess several curved internal walls. Tubular protuberances project from the ellipsoids or spheres. Rarely, long halloysite tubes outgrow from an ellipsoid. Based on the chemistry, morphol-

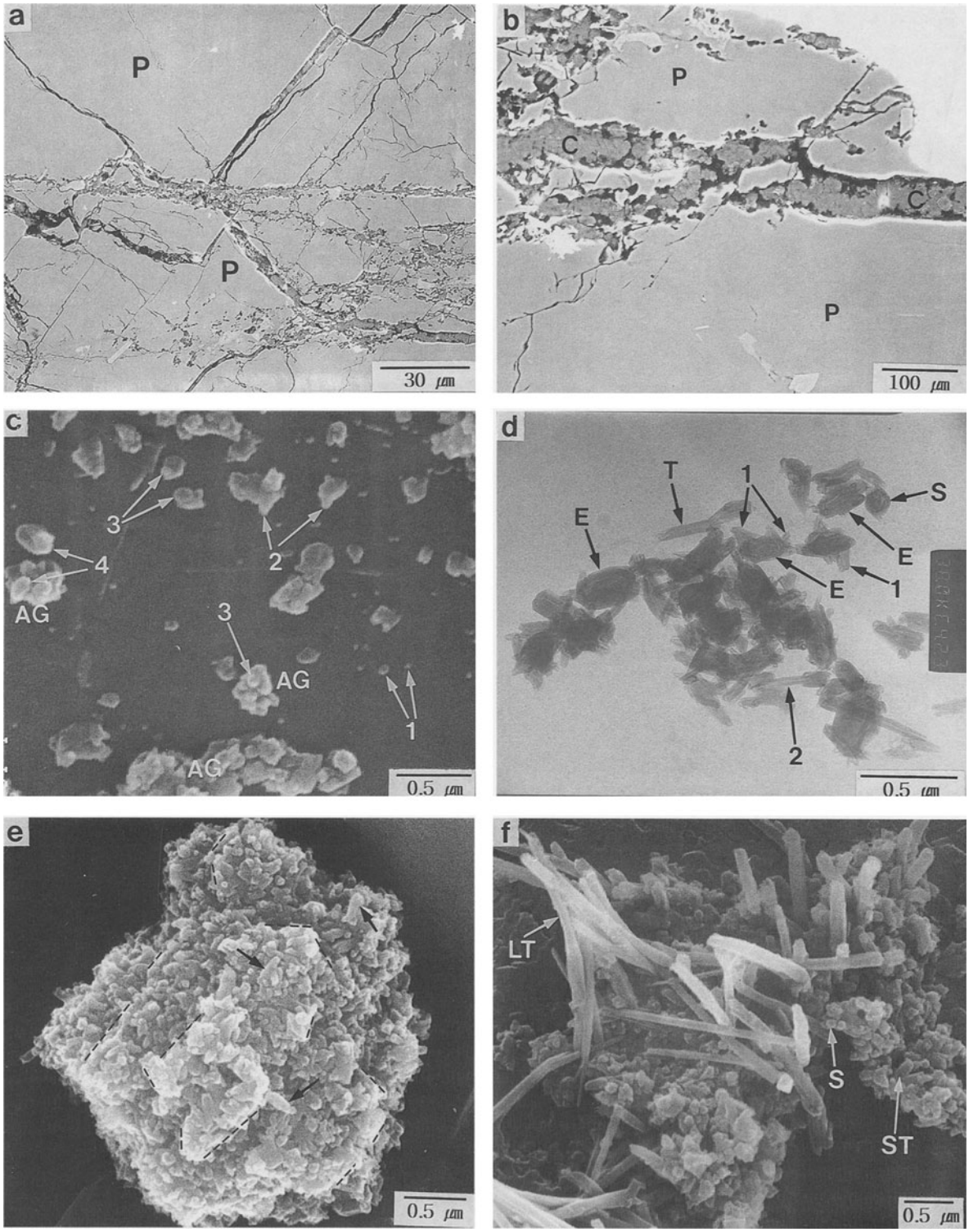

Figure 2. Electron micrographs of least-weathered anorthosite (sample R1). a) SEM photograph of thin section; widened microfractures in plagioclase (P). b) Magnified photograph of the lower right area in (a); clays (C) in the microfractures. c) SEM photograph of scattered kaolin mineral grains of varying sizes and their aggregates (AG) on plagioclase surface; very small embryonic grains (arrow 1), protuberances (arrow 2), overgrowing spheres (arrow 3) and ellipsoids (arrow 4). d) TEM photograph of kaolin minerals; ellipsoids (E), tubes (T) and spheres (S). Note tubular protuberances (arrow 1) and outgrowing long tubes (arrow 2). e) SEM photograph of globular aggregate of halloysite; stacked surfaces (boundaries are indicated by broken lines) and flat-lying tubes (arrows). f) SEM photograph of halloysite aggregate; long tubes (LT), short tubes (ST) and spherical overgrowths on plate (S).

https://doi.org/10.1346/CCMN.1998.0460306 Published online by Cambridge University Press

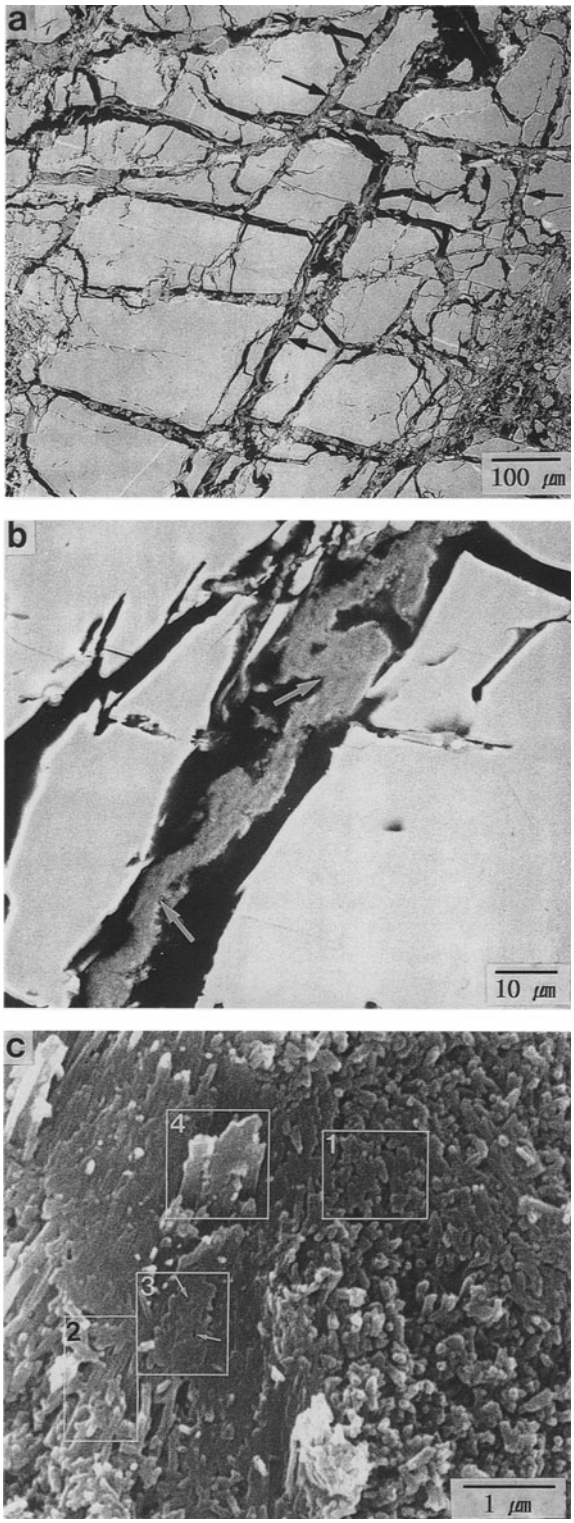

Figure 3. SEM photographs of slightly weathered anorthosite (sample R2). a) Thin section: halloysite fillings (arrows) and voids (black) in the widened microfractures of plagioclase. b) Thin section: wrinkled halloysite mass (arrows) and voids (black). c) Raw sample: coalescence of tubes into a plate. Box 1, coalescing short tubes in a plane; box 2, coalescing long tubes; box 3, a plate with voids (arrows); and box 4, complete plates.

ogy and internal structure, the ellipsoids are identified as halloysite. Thus, the kaolin mineral grains in Figure 2c are mostly halloysite ellipsoids with common tubular or spherical protuberances. Ellipsoids, spheres and tubes constitute together large globular aggregates (Figure 2e), which might be a more developed form of the globular aggregate in Figure 2c. The long axes of halloysite ellipsoids or tubes in the aggregate are not randomly oriented, but roughly parallel with plagioclase surfaces. Several stacked surfaces consisting of flat-lying ellipsoids and tubes are observed in the aggregate. Long tubes often rise from the aggregates consisting of spheres and short tubes (Figure 2f).

SAMPLE R2. A SEM photograph of a thin section shows the increased voids and extensive kaolin fillings in the microfractures (Figure 3a). The plagioclase surfaces are still straight and lack deep etch pits, implying weak dissolution of plagioclase. The kaolin fillings often occur as compact, homogeneous and wrinkled masses spaced from the fracture walls (Figure 3b). Wrinkling of compact halloysite aggregates was reported in a previous study (Jeong and Kim 1993). A magnified SEM photograph of raw samples shows the intergrading textures from flat-lying halloysite mesh to larger plate. Short and long halloysite tubes are interconnected and matted in a plane with interstitial voids, and grade through porous incomplete plates to larger solid plates at the center of the aggregate (Figure 3c).

SAMPLE R3. A SEM photograph of a thin section displays thick kaolin fillings in microfractures and deep, serrated etch-pits on the plagioclase surfaces, implying intense dissolution (Figure 4a). A magnified SEM photograph (Figure 4b) shows that the kaolin fillings are no longer compact and homogeneous compared to those in Figure 3b, but tend to form numerous small embryonic vermicular clusters or several well-developed long vermicular clusters up to 0.5 μm wide and 25 μm long. An SEM photograph of another area of the thin section shows more voids, implying more advanced weathering (Figure 4c). A magnified photograph (Figure 4d) shows that porous kaolin aggregates are separated from the deeply etched plagioclase and wrinkled in the same manner as that in Figure 3b. They are composed of abundant, well-developed vermicular clusters. The long axes of the clusters are arrayed roughly perpendicular to the fracture direction (Figure 4d).

High-magnification SEM photographs of raw samples show the detailed surficial features of the vermicular clusters observed in the thin section. The large vermicular clusters have highly rugged surfaces which consist of matted tubes, branched tubes and abundant irregular plates of varying sizes (Figure 5a). The irregular outlines of the plates are due to tubular protuberances, suggesting diverse intergrades between tube and plate. Small irregular plates are indistinguishable from the branched tubes. Figure 5b shows a long

https://doi.org/10.1346/CCMN.1998.0460306 Published online by Cambridge University Press

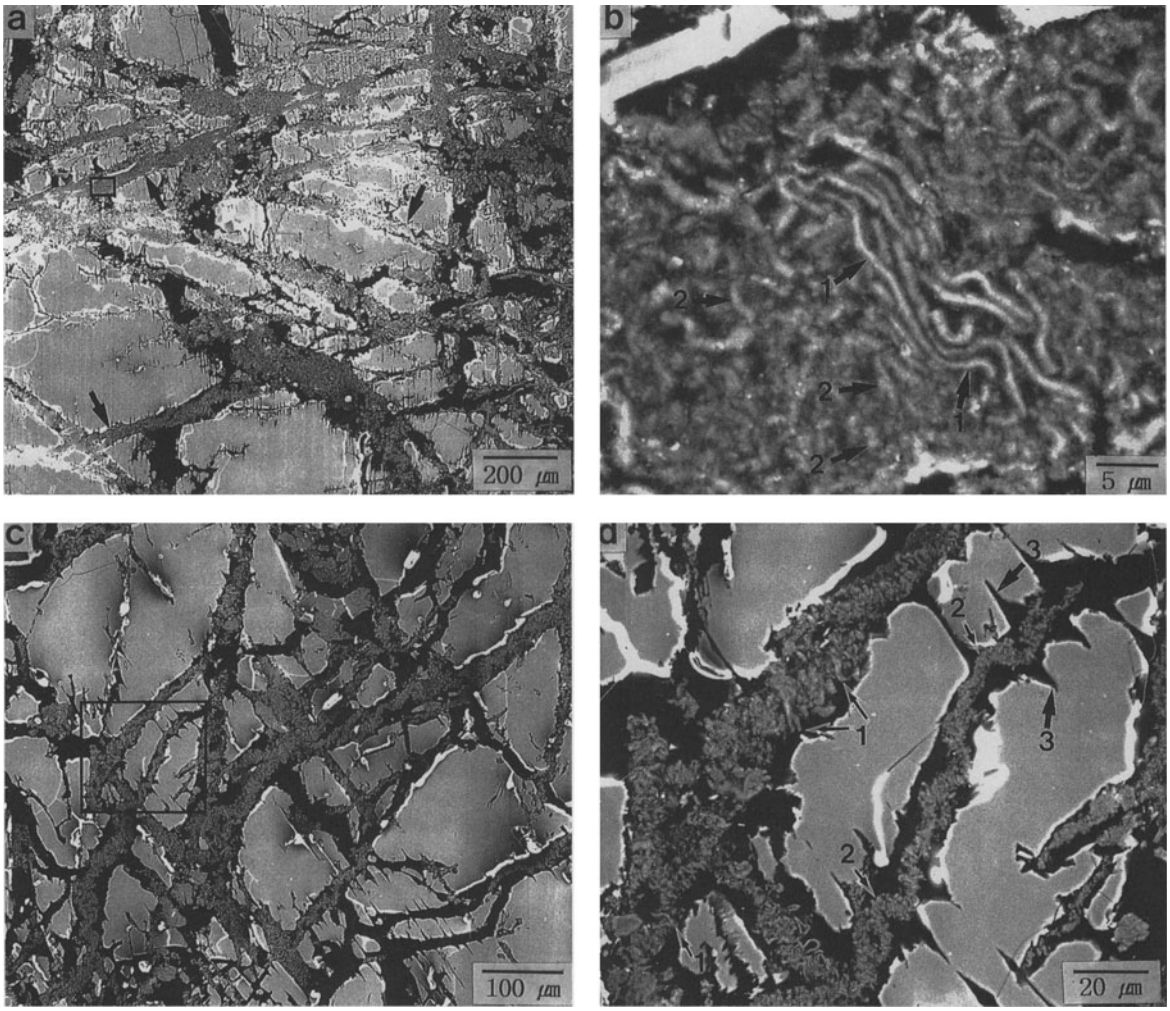

Figure 4. SEM photographs of thin sections of moderately weathered anorthosite (sample R3). a) Kaolin fillings (arrows) in the microfractures of plagioclase and abundant etch pits on the surface of plagioclase. b) Magnified photograph of the box in (a); long well-formed vermicular clusters (arrow 1) among embryonic vermicular clusters (arrow 2). c) Kaolin fillings and abundant voids in more-weathered area. d) Magnified photograph of the box in (c) showing kaolin fillings. Arrow 1, vermicular grains arrayed in parallel with each other and roughly perpendicular to the microfracture direction; arrow 2, wrinkling of kaolin aggregates; and arrow 3, etch pits.

vermicular stack rising from halloysite aggregates. A magnified photograph (Figure 5c) shows that small embryonic ellipsoids or short tubes grow at the top of the stack, while long tubes grow out from the side.

TEM photographs of raw samples show irregular plates with long tubular protuberances (Figure 6a) and vermicular clusters of kaolin minerals (Figures 6b and 6c). The clusters in Figure 6b appear to be vermicular stacks of plates with thick halloysite overgrowths. Those in Figure 6c are apparently well-developed long vermicular stacks of plates growing out from the aggregate of kaolin minerals, probably halloysite tubes. The effect is very similar to those shown in Figures 5b and 5c.

Respective kaolin minerals are difficult to identify because they are similar in chemistry and structure. Morphological identification is not sufficient (Churchman and Gilkes 1989; Bailey 1990), but under SEM and TEM, it is commonly used as the main criterion distinguishing kaolinite from halloysite (Robertson and Eggleton 1991; Singh and Gilkes 1992). Although rare iron-rich halloysites can occur as plates (Kunze and Bradley 1964; Noro 1986), halloysite commonly shows a curved morphology (spheres, tubes and crinkled sheets). Previous electron microprobe data for the halloysite aggregates (Jeong 1992) show that halloysite in Sancheong kaolin deposits consists mostly of Al and Si with minor Fe (Fe_2O_3 mostly below 0.6 wt%). Therefore, plates or their stacks in the micrographs are ascribed to kaolinite. This is supported by the fact that the high kaolinite content in sample R3 estimated by XRD is consistent with the abundant ver-

https://doi.org/10.1346/CCMN.1998.0460306 Published online by Cambridge University Press

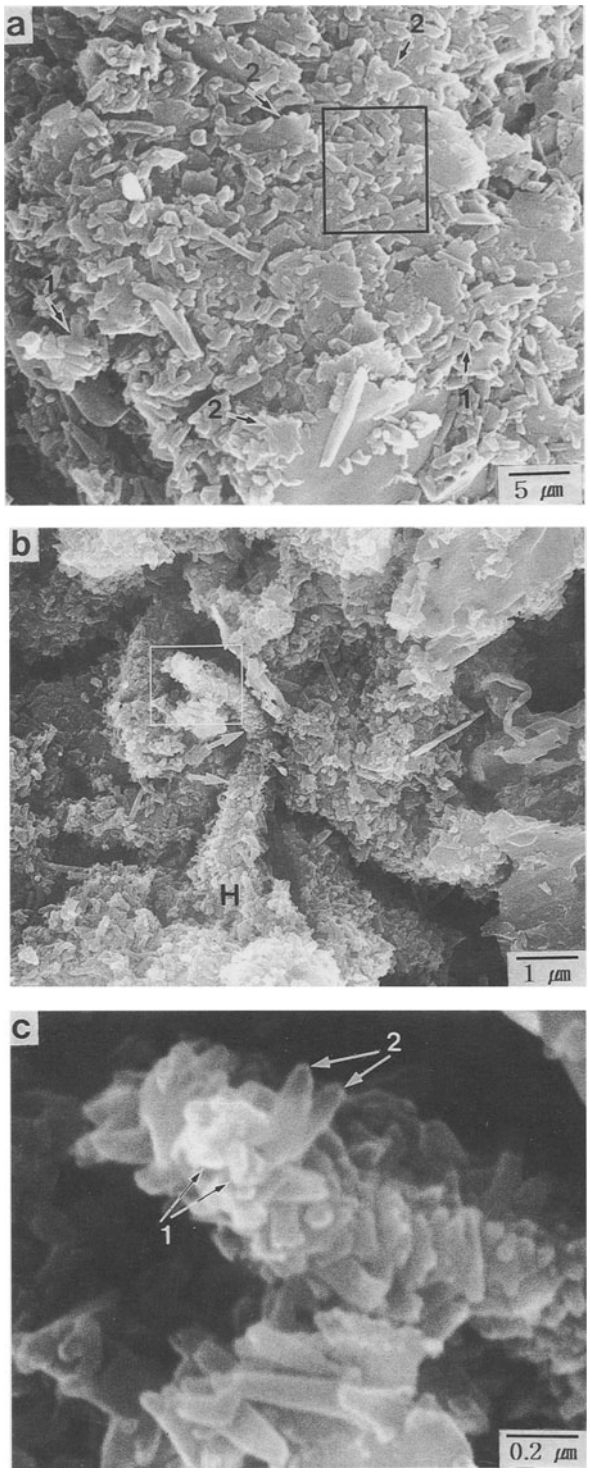

Figure 5. SEM photographs of raw samples of moderately weathered anorthosite (sample R3). a) The surface of a vermicular cluster; tubes matted in a plane (box), branched tubes (arrow 1) and plates with protuberances (arrow 2). b) Long vermicular kaolin clusters (arrow) rising from halloysite aggregate (H). c) Magnified photograph of the box in (b); embryonic halloysites (arrow 1) growing at the end of the vermicular stack and long tubes (arrow 2) protruding from the vermicular stack.

micular stacks of plates observed under SEM. The vermicular stacks in the SEM and TEM micrographs observed in this study are identified as vermicular kaolinite with abundant halloysite overgrowths.

DISCUSSION

Formation of Vermicular Kaolinite from Halloysite Aggregates

HALLOYSITE AGGREGATES. Halloysite initially nucleates as scattered tiny embryonic grains and gradually grows into larger ellipsoids and spheres (Figure 2c). Occasionally, the continued growth of ellipsoids and spheres proceeds via short tubes to long tubes (Figure 2f). New small halloysite grains repeatedly project from the first grain, forming protuberances around it and growing to further ellipsoids and short tubes (Figure 2c). Successive generation of halloysite grains results in globular aggregates (Figures 2c and 2e). The growth by repeated projection suggests that halloysite grains are at least partially interconnected, thus giving considerable internal consistency to the aggregates. Halloysite aggregates are not easily dispersed by intense ultrasonic agitation, suggesting their considerable rigidity (Jeong and Kim 1992). The stacked surfaces in Figure 2e suggest that the globular aggregates might result from the accumulation of successively formed networks of flat-lying halloysite ellipsoids and tubes. The networks are not completely separated but partially interconnected. Growing globular aggregates (Figure 2e) are merged into extensive planar masses, which are wrinkled after detachment from dissolving plagioclase (Figure 3b) by the continued growth of halloysite tubes in the aggregate, as suggested by Jeong and Kim (1993).

VERMICULAR KAOLINITE. Vermicular kaolinites have been frequently reported in literature dealing with weathering and sedimentary environments. They may be formed by the weathering of mica (Fitzpatrick 1984; Banfield and Eggleton 1988; Singh and Gilkes 1992; Jeong et al. 1995) or of feldspar weathering (Keller 1977). Keller (1977) suggested the direct formation of vermicular kaolinite from solution during feldspar weathering. This study shows that vermicular kaolinite could be formed via halloysite precursors rather than through direct formation from solution. A series of SEM photographs of thin sections of sample R1 (Figure 2b), sample R2 (Figures 3a and 3b) and sample R3 (Figures 4a, 4b, 4c and 4d) collectively suggest that the early-formed halloysite aggregates in sample R1 are gradually converted into vermicular kaolinites in sample R3 with progressive weathering. Figure 3c suggests the process whereby halloysite aggregates are converted into kaolinite plates. Short or long tubes in the outer part of halloysite aggregates are interconnected to form a network. Interstitial spaces among the halloysite grains are gradually filled by

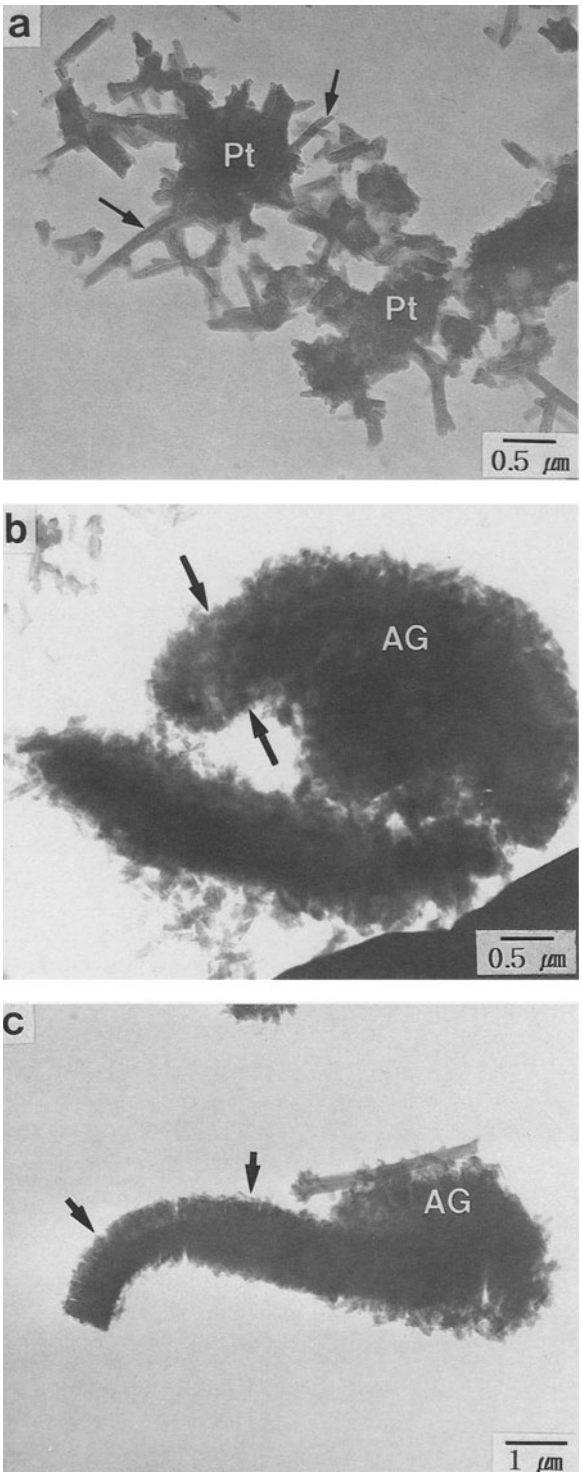

Figure 6. TEM photographs of vermicular kaolin mineral aggregates. a) Plates (Pt) with outgrowing tubular protuberances (arrows). b) Vermicular kaolin mineral aggregates (AG). Note the protrusion of vermicular kaolinite from AG (arrows). c) A long vermicular kaolinite protrusion (arrows) from AG.

continued growth from the inner part of the aggregate to form an incomplete plate with minute remnant voids. Finally all the voids disappear to form a larger plate at the center of aggregate (Figure 3c). Successive coalescence and transformation of adjacent halloysite networks into plates within aggregates may result in the vermicular stacks of kaolinite plates. Successive addition of halloysites on the previously formed plates and their subsequent transformation into kaolinite plates result in longer vermicular stacks of kaolinite (Figures 5b and 5c). Plates with tubular protuberances or branched tubes, as shown in Figure 5a, are interpreted to be intergrades between halloysite tubes and kaolinite plates formed during the conversion of halloysite to kaolinite. Banfield (1985) suggested that platy kaolinite could be formed by the coalescence of halloysite tubes.

A possible mechanism of the conversion is simultaneous solution and precipitation (Tsuzuki and Kawabe 1983; Steefel and Van Cappellen 1990). However, this study failed to find any texture attributable to halloysite dissolution. Considering the structural and chemical similarity between halloysite and kaolinite, a chemical reaction including complete structural decomposition and reconstruction would be difficult to envisage in the low-temperature weathering environments. Churchman and Gilkes (1989) suggested that halloysite tubes could be altered to kaolinite via dehydrated halloysite in solid state by prolonged dehydration. In their study of kaolin pseudomorphs after muscovite, Singh and Gilkes (1992) reported the reverse phenomenon, where platy kaolinite converts into tubular halloysite via solid-state transformation. The present study suggests that the major conversion mechanism, on the basis of the observed microtextures, is a solid-state transformation of interconnected halloysite grains into larger kaolinite plates by coalescence. The low crystallinity and very broad basal peak for the kaolinites also supports the view that they are derived from halloysite through solid-state transformation. However, this mechanism encounters the difficult problem of how the curved halloysite layers would be converted into platy kaolinite layers. It is suggested that the curved layers are probably flattened by partial ruptures or weak dissolution rather than complete recrystallization. The general process of formation of vermicular kaolinite from halloysite aggregate is schematically described in Figure 7.

Thermodynamic and Kinetic Considerations on Coexisting Halloysite and Kaolinite

Conversion of halloysite to kaolinite is consistent with thermodynamic considerations. The Gibbs free energy of formation of halloysite is about 4 kcal/mol higher than that of kaolinite (Robie and Waldbaum 1968; Robie et al. 1978; Anovitz et al. 1991). Therefore, halloysite is metastable compared to coexisting

https://doi.org/10.1346/CCMN.1998.0460306 Published online by Cambridge University Press

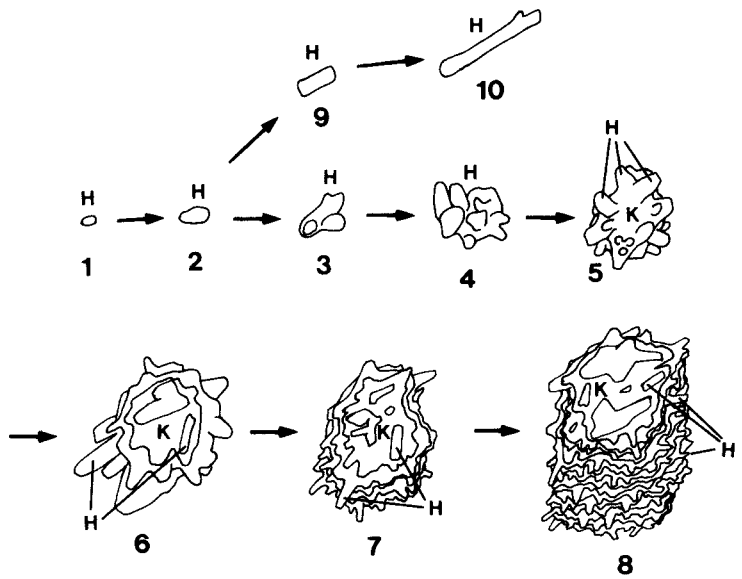

Figure 7. Schematic diagram showing the formation process of vermicular kaolinite from halloysite aggregate: 1, halloysite embryo; 2, halloysite ellipsoid; 3, growth of new ellipsoids, spheres and tubes; 4, interconnected halloysite aggregate formed by repeated growth; 5, interconnected halloysite grains coalesced into kaolinite plate at the center; 6, irregular kaolinite plate with tubular halloysite overgrowths and their subsequent transformation into plates by coalescence; 7–8, long vermicular stacks of kaolinite plates; and 9–10, halloysite ellipsoid growing into long tubes. Key: H = halloysite; K = kaolinite.

kaolinite. In low-temperature geological environments, metastable equivalents generally precipitate more rapidly than stable minerals because nucleation of more soluble minerals with high surface free energy is kinetically easier (Morse and Casey 1988; Stumm 1992). However, metastable minerals are ultimately transformed to stable minerals with aging. Halloysite precipitates as a metastable precursor to relatively stable kaolinite. However, the aggregates consisting of soluble, fine halloysite grains are unstable and replaced by kaolinite with progressive weathering. Kinetic simulation carried out by Steefel and Van Cappellen (1990) suggested that halloysite precipitates at an early stage and is replaced by kaolinite with aging. The textural evidence in this study is consistent with their simulation results, but this study suggests that solid-state transformation is a more likely conversion mechanism than solution-precipitation. Robertson and Eggleton (1991) and Singh and Gilkes (1992) described conversion of kaolinite to halloysite, but did not explain the origin of hydration in this process. Dehydration of halloysite is known to be an irreversible process without the aid of intercalation (Churchman 1970). Therefore, it is not expected that kaolinite would be spontaneously hydrated in the natural state to form halloysite. Acceptance of the formation of halloysite via hydration of kaolinite in the natural environment awaits more evidence and explanations.

Kaolinite formation is not followed by an immediate decrease of halloysite content. The XRD data suggest that halloysite content steadily increases in spite of the formation of kaolinite. Vermicular grains with halloysite overgrowths (Figures 5a, 5c, 6b and 6c) suggest that halloysites precipitate continuously as a metastable precursor on the surface of vermicular grains, concurrently with their transformation into kaolinite. Metastable halloysite and stable kaolinite can temporarily coexist in the relatively recent weathering profiles of Sancheong kaolin deposits.

SUMMARY AND CONCLUSION

Previous literature frequently reports an association between halloysite aggregates and vermicular kaolinite, but little attention has been given to their genetic relations. SEM observations on a series of partially weathered anorthosites demonstrate the genetic sequence between coexisting halloysite and vermicular kaolinite in anorthosite weathering profiles. It is shown that vermicular kaolinite could form from halloysite during the weathering of feldspar. Early-formed halloysite aggregates are converted into long vermicular kaolinites by coalescence with progressive weathering. Microtextures suggest that solid-state transformation is the major mechanism of halloysite to kaolinite conversion, instead of solution-precipitation. Kaolinite formation is accompanied by the continued precipitation of halloysite as a metastable precursor. In the weathering profiles far from equilibrium, metastable halloysite can coexist with kaolinite.

ACKNOWLEDGMENTS

The author thanks G. J. Churchman and an anonymous reviewer for their critical reviews and J. F. Banfield for read-

ing the early manuscript. S. J. Kim is thanked for introducing the author to clay mineralogy. This work was supported by the Basic Science Research Institute Program, Ministry of Education, Korea (project No. BSRI 96-5402).

REFERENCES

Anovitz LM, Perkins D, Essene EJ. 1991. Metastability in near-surface rocks of minerals in the system Al_2O_3-SiO_2-H_2O. Clays Clay Miner 39:225–233.

Bailey SW. 1990. Halloysite—A critical review. In: Farmer VC, Tardy Y, editors. Proc Int Clay Conf; Strasbourg, France. Sci Geol Mem 86:89–98.

Banfield JF. 1985. The mineralogy and chemistry of granite weathering [M.Sc. thesis]. Canberra, Australia: Australian National Univ. 130 p.

Banfield JF, Eggleton RA. 1988. Transmission electron microscope study of biotite weathering. Clays Clay Miner 36: 47–60.

Banfield JF, Eggleton RA. 1990. Analytical transmission electron microscope studies of plagioclase, muscovite, and K-feldspar weathering. Clays Clay Miner 38:77–89.

Brindley GW. 1980. Order–disorder in clay mineral structures. In: Brindley GW, Brown G, editors. Crystal structures of clay minerals and their X-ray identification. London: Mineral Soc. p 125–195.

Chukhrov FV, Zvyagin BB. 1966. Halloysite, a crystallochemically and mineralogically distinct species. In: Heller L, Weiss A, editors. Proc Int Clay Conf, vol. 1; 1966; Jerusalem, Israel. Jerusalem, Israel: Programs of Science in Translation. p 11–25.

Churchman GJ. 1970. Interlayer water in halloysite [Ph.D. thesis]. Dunedin, New Zealand: Univ of Otago. 270 p.

Churchman GJ, Gilkes RJ 1989. Recognition of intermediates in the possible transformation of halloysite to kaolinite in the weathering profiles. Clay Miner 24:579–590.

Churchman GJ, Whitton JS, Claridge GGC, Theng BKG. 1984. Intercalation method using formamide for differentiating halloysite from kaolinite. Clays Clay Miner 32:241–248.

Fitzpatrick EA. 1984. Micromorphology of soils. New York: Chapman and Hall. 433 p.

Gilkes RJ, Suddhiprakarn A, Armitage TM. 1980. Scanning electron microscope morphology of deeply weathered granite. Clays Clay Miner 28:29–34.

Hinckley DN. 1993. Variability in "Crystallinity" values among the kaolin deposits of the coastal plain of Georgia and South Carolina. Clays Clay Miner 11:229–235.

Huang WH. 1974. Stabilities of kaolinite and halloysite in relation to weathering of feldspars and nepheline in aqueous solution. Am Mineral 59:365–371.

Hughes JC, Brown G. 1979. A crystallinity index for soil kaolins and its relation to parent rock, climate and soil maturity. J Soil Sci 30:557–563.

Jeong GY. 1992. Mineralogy and genesis of kaolin in the Sancheong district, Korea [Ph.D. thesis]. Seoul, Korea: Seoul National Univ. 325 p.

Jeong GY, Kim SJ. 1989. 7 Å phase in the Sancheong kaolin: 7 Å-halloysite or kaolinite? J Mineral Soc Korea 2:18–25.

Jeong GY, Kim SJ. 1992. Mineralogy of size fractions in Sancheong kaolin and its origin. J Mineral Soc Korea 5: 22–31.

Jeong GY, Kim SJ. 1993. Boxwork fabric of halloysite-rich kaolin formed by weathering of anorthosite in Sancheong area, Korea. Clay Clay Miner 41:56–65.

Jeong GY, Kim SJ. 1994. Genesis of kaolin in the Sancheong district, Korea: Mineralogical and textural study. J Geol Soc Korea 30:262–283.

Jeong GY, Kim SJ, Kim YH, Cho HG. 1995. Kaolinite formation by weathering of biotite in Sancheong kaolin. J Mineral Soc Korea 8:37–45.

Jeong JG, Lee SM. 1987. Regional metamorphism of anorthositic rocks in Hadong-Sancheong area. In: Kim HS, editor. Memoirs in celebration of the sixtieth birthday of Professor Sang Man Lee. Seoul, Korea: Seoul National Univ. p 87–106.

Keller WD. 1977. Scan electron micrographs of kaolins collected from diverse environments of origin—IV. Georgia kaolin and kaolinizing source rocks. Clays Clay Miner 25: 311–345.

Keller WD, Cheng H, Johns WD, Meng C-S. 1980. Kaolin from original Kauling (Gaoling) mine locality, Kiangsi province, China. Clays Clay Miner 28:97–104.

Korea Mining Promotion Corporation. 1995. Mining summary of Korea. Seoul, Korea: Korea Mining Promotion Corp. 417 p.

Krauskopf KB, Bird DK. 1995. Introduction to geochemistry. New York: McGraw-Hill. 647 p.

Kunze GW, Bradley WF. 1964. Occurrence of a tabular halloysite in a Texas soil. Clays Clay Miner 12:523–527.

Kwon ST, Jeong JG. 1990. Preliminary Sr-Nd isotope study of the Hadong-Sanchung anorthositic rocks in Korea: Implication for their origin and for the Precambrian tectonics. J Geol Soc Korea 26:341–349.

Morse JW, Casey WH. 1988. Ostwald process and mineral paragenesis in sediments. Am J Sci 288:537–560.

Nagasawa K. 1978. Kaolin minerals. In: Sudo T, Shimoda S, editors. Clays and clay minerals of Japan. Tokyo, Japan: Kodansha. p 189–219.

Newman ACD, Brown G. 1987. The chemical constitution of clays. In: Newman ACD, editor. Chemistry of clays and clay minerals. London: Mineral Soc. p 1–128.

Noro H. 1986. Hexagonal platy halloysite in an altered tuff bed, Komaki city, Aichi Prefecture, Central Japan. Clay Miner 21:401–415.

Parham WE. 1969. Formation of halloysite from feldspar: Low temperature artificial weathering versus natural weathering. Clays Clay Miner 17:13–22.

Robertson IDM, Eggleton RA. 1991. Weathering of granitic muscovite to kaolinite and halloysite and of plagioclase-derived kaolinite to halloysite. Clays Clay Miner 39:113–126.

Robie RA, Waldbaum DR. 1968. Thermodynamic properties of minerals and related substances at 298.15 °K (25 °C) and one atmosphere (1.013 bars) pressure and at higher temperatures. US Geol Surv Bull 1259. 256 p.

Robie RA, Hemingway BS, Fisher JR. 1978. Thermodynamic properties of minerals and related substances at 298.15 °K (25 °C) and 1 bar (10^5 pascals) pressure and at higher temperatures. US Geol Surv Bull 1452. 456 p.

Singh B, Gilkes RJ. 1992. An electron optical investigation of the alteration of kaolinite to halloysite. Clays Clay Miner 40:212–229.

Steefel CI, Van Cappellen P. 1990. A new kinetic approach to modeling water-rock interaction: The role of nucleation, precursors, and Ostwald ripening. Geochim Cosmochim Acta 54:2657–2677.

Stumm W. 1992. Chemistry of the solid-water interface. New York: J. Wiley. 428 p.

Tsuzuki Y, Kawabe I. 1983. Polymorphic transformations of kaolin minerals in aqueous solutions. Geochim Cosmochim Acta 47:59–66.

Weaver CE, Pollard LD. 1973. The chemistry of clay minerals. Amsterdam, Holland: Elsevier. 213 p.

(Received 18 February 1997; accepted 9 September 1997; Ms. 97-018)